

Laser refrigeration, alignment and rotation of levitated Yb^{3+} :YLF nanocrystals

A. T. M. Anishur Rahman & P. F. Barker*

Department of Physics & Astronomy, University College London,

*Gower Street, WC1E 6BT, London, UK. *E-mail: p.barker@ucl.ac.uk.*

The ability to cool and manipulate levitated nanoparticles in vacuum is a promising tool for exploring macroscopic quantum mechanics^{1,2}, precision measurements of forces³ and non-equilibrium thermodynamics^{4,5}. The extreme isolation afforded by optical levitation offers a low noise, undamped environment that has to date been used to measure zeptonewton forces³, radiation pressure shot noise⁶, and to demonstrate centre-of-mass motion cooling^{7,8}. Ground state cooling, and the creation of macroscopic quantum superpositions, are now within reach, but control of both the centre-of-mass and internal temperature is required. While cooling the centre-of-mass motion to micro Kelvin temperatures has now been achieved, the internal temperature has remained at or above room temperature. Here we realise a nanocryostat by refrigerating levitated Yb^{3+} :YLF nanocrystals to 130 K using anti-Stokes fluorescence cooling, while simultaneously use the optical trapping field to align the crystal to maximise cooling.

Laser cooling the centre-of-mass motion of atoms to ultra-cold temperatures has led to a revolution in physics over the last thirty years. This has allowed the creation of quantum gases, the study of quantum many body physics and novel states of matter⁹. In more recent years cooling of more complex systems including molecules and even levitated nanoparticles^{7,8} has been demonstrated.

Laser cooling (refrigeration) of solid materials has, despite first predictions¹⁰ in 1929, made somewhat slower progress. Like the well known process of Doppler cooling⁹, blue shifted spontaneous emission of photons with respect to the excitation wavelength leads to cooling. The difference is that unlike Doppler cooling of atoms, it is the internal temperature of the solid that is lowered by converting phonons to higher energy photons, thereby decreasing both the temperature and entropy of the system^{11,12}. Last year cryogenic temperatures (90 K) were realised for the first time using this technique¹³ in a bulk crystal of $\text{Yb}^{3+}:\text{YLF}$, while the first demonstration¹⁴ in 1995 cooled $\text{Yb}:\text{ZBLAN}$ glass by 0.3 K.

This type of cooling opens up a wide range of applications, where in contrast to conventional cryogenic methods, heat transfer from the solid to the environment occurs by fluorescence emission *without* physical contact. Such a mechanism now offers cryogenic cooling within enclosed spaces without the need for electrical connections or conductive materials, with clear applications within a vacuum or space environment¹². Recently, laser refrigeration on a microscopic scale has been demonstrated in optical tweezers experiments using $\text{Yb}^{3+}:\text{YLF}$ crystals in water by measuring cold Brownian motion¹⁵. Here the water temperature was reduced by 20 K, with the final temperature limited by the high conductive heat transfer of liquid water. Refrigeration on the microscale in such biophysical environments is seen as a promising tool for exploring the temperature effects of physiological processes.

We report on the refrigeration of levitated 10 % $\text{Yb}^{3+}:\text{YLF}$ nanocrystals to temperatures as low as 130 K using a single beam optical dipole trap within a low pressure environment. The same light field that traps also leads to anti-Stokes refrigeration of the crystal. The temperature of the crystal is observed by both measuring the changes in fluorescence emitted from the nanocrystal as a function of laser wavelength, and also by the temperature-dependent damping of the motion of the nanocrystal. We show that temperature can be controlled over a wide range (130 - 300 K) using different trapping laser wavelengths, while the laser polarization allows us to control the orientation of the trapped crystal and maximise its cooling.

A schematic of our experiment for levitated anti-Stokes refrigeration is shown in Fig. 1a. A laser beam is tightly focussed into a diffraction limited spot by a 0.80 numerical aperture microscope objective to form a 3D optical dipole trap. The energy level diagram of Yb^{3+} in YLF is shown in Fig. 1b, while panel c shows the recorded blue-shifted fluorescence from a levitated $\text{Yb}^{3+}:\text{YLF}$ nanocrystal. The fluorescence is collected using the same trapping objective

and is sent to a spectrometer. A lens (Fig. 1d) collects the transmitted and scattered light from a levitated nanocrystal, which is directed to photodiodes that measure the motions of the trapped crystal.

The energy level structure of Yb^{3+} embedded in the YLF consists of an $F_{7/2}$ ground state and a $F_{5/2}$ excited state, each of which is split into a manifold of non-degenerate states by the crystal field^{16,17}. The radiative lifetime of the excited state in the bulk crystal is on the order of milliseconds¹⁶ and there is no significant non-radiative relaxation^{12,18}. Rapid phonon coupling between the levels in each electronic state occurs over picosecond time-scales, rapidly thermalising the population in these levels. Anti-Stokes refrigeration occurs via optical excitation at a wavelength that is resonant with the bandgap between the two electronic states at approximately 1020 nm (as shown in figure 1b). Due to the rapid thermalisation in the upper state fluorescence from the excited state is blue-shifted with respect to the excitation wavelength. This reduces the average phonon energy and the lattice temperature of the levitated Yb^{3+} :YLF nanocrystal.

Figure 1c shows the fluorescence spectra (blue and red lines) from the coldest levitated Yb^{3+} :YLF nanocrystal from our experiment. This was levitated using 1031 nm linearly polarised light. When trapping at high laser powers 50 - 200 mW (irradiance of $0.83 - 3.5 \times 10^{11} \text{ Wm}^{-2}$ at the focus), the typical spectral profile observed is shown by the blue curve. This profile corresponds to the crystal's c -axis oriented parallel to the polarization of the optical field (E). In this orientation the maximum absorption and cooling has been observed in bulk crystals. When the trapping power is lowered to below 50 mW, the spectral profile changes to that shown by the red curve. This profile corresponds to an orientation of the crystal's a -axis parallel to the laser polarisation. This well defined alignment is in contrast to the random alignment of the crystal axes when the nanocrystals are deposited on a microscope coverglass. This type of alignment has been observed in the trapping of birefringent crystals in aqueous media¹⁹. Figure 1c also contains the spectrum from a nanocrystal deposited on a SiO_2 coverglass in $c//E$ orientation and illuminated by the 1031 nm laser with the same power used for levitation.

We determine the temperature of the trapped nanocrystals from their fluorescence spectra which are directly related to the relative population of the E_5 , E_6 and E_7 levels in the upper $F_{5/2}$ electronic state via the Boltzmann distribution^{20,21}(see methods for details). Figures 2a&b show high resolution spectra that clearly identify Yb^{3+} transitions¹⁶ on 1031 nm and 1064 nm levitation, respectively. It is obvious that the relative heights of transitions originating from E_5 level are higher for the 1031 nm levitation when compared to 1064 nm. This indicates that the 1031 nm levitated crystal is at a significantly lower temperature than the crystal levitated with 1064 nm light. Figure 2c is the spectrum obtained from a nanocrystal that is deposited on a SiO_2 coverglass and illuminated by the 1031 nm laser with the same power used for levitation. We assume that the crystal is at room temperature as it is directly

in contact with the coverglass. This was further confirmed by reducing the laser power by two orders of magnitude which shows little change in the relative heights of the spectral peaks.

Figure 2d shows the temperatures of 13 particles trapped using 1031 nm and 1064 nm light. In all cases the trapping power at the focus of the microscope objective was 200 mW. We note that the temperature of the particle remains approximately constant for all trapping powers and pressures (1000 mB - 40 mB) considered here. Although there is some variation between the temperature of particles trapped by 1031 nm light we find an average internal temperature of 167 K. The lowest temperature recorded in our experiment is ≈ 130 K as shown in the lower resolution spectrum of Fig. 1c. For the fewer particles trapped at 1064 nm we find an average temperature of 260 K which is consistent with predictions¹⁸. Significantly lower temperatures will be obtained using trapping light near 1020 nm where the minimum temperature has been achieved in bulk crystals. To compare the temperatures that can be achieved on the same particle at different trapping wavelengths we initially trapped a particle using 1031 nm light and recorded spectra. We then moved the particle to the 1064 nm trap by slowly decreasing the 1031 nm intensity while increasing the 1064 nm power. The temperature of this particle at both wavelengths is shown as particle number 2 in Fig. 2d.

The natural birefringence and shape induced birefringence of the asymmetric trapped $\text{Yb}^{3+}:\text{YLF}$ nanocrystals allow us to observe rotation and alignment of the particles via the transfer of angular momentum from the light. Figure 4a shows a plot of the power spectral density (PSD) under linearly polarised trapping light at ≈ 500 mB. This leads to a type of rotational simple harmonic motion when the nanocrystal aligns itself with the polarisation axis of the trapping beam²². Figure 4b is a plot of the PSD recorded at the same pressure when the circularly polarized (CP) light is used to trap the nanocrystal^{23,24}. We can tune between these two types of motion by changing the polarization of the trapping beam using a $\frac{\lambda}{4}$ waveplate. In addition to the usual rotational motion due to the inherent birefringence, absorption of CP light by Yb^{3+} ions or non-uniform radiation pressure forces on asymmetric nanocrystals²⁵ could also transfer angular momentum. Figure 4c is a plot of the observed frequency modulation of the transmitted trapping signal as a function of waveplate angle. For rotational motion induced by CP light the rotation frequency increases for decreased gas damping. However, for linearly polarised light the frequency of the pendular motion does not change with damping as is confirmed by the plot in Fig. 4d.

When the crystal is levitated in gas, refrigeration leads to cooling of the surrounding gas molecules and also to a modification in the local gas viscosity. The resultant temperature dependent damping rate of the translational motion due to both hot and cold Brownian motion of a trapped particle has been used to measure temperature in liquids and gases^{5,15,26}. We utilise this effect on the pendular motion for the first time. For air at the temperatures and pressures we use, the viscosity and damping rate scales²⁷ with temperature as $T^{1/2}$. The change in damping rate with

temperature in different wavelength traps for the same particle is used to measure particle temperature. Figures 3a&b are the PSDs of a single particle (number 2 in Fig. 2d) trapped in 1031 nm and 1064 nm wavelength light at a pressure of 600 mB. The PSDs shown in Fig. 3 contain fits to the data that include both the translational degree of freedom (green, low freq. regime) and the pendular motion (purple, main peak). The damping rate derived from the fit to the pendular motion using 1031 nm light was found to be $\Gamma_{1031}^p/2\pi = 13.94 \pm 0.85$ kHz and $\Gamma_{1064}^p/2\pi = 17.03 \pm 0.48$ kHz for the 1064 nm trap giving a damping ratio of $R_p = \Gamma_{1031}^p/\Gamma_{1064}^p = 0.82 \pm 0.05$. For the translational motion we determine a damping ratio of $R_t = 0.74 \pm 0.1$. Assuming that the internal temperature of the particle in the 1064 nm beam is $T_0 = 255$ K, obtained from our fluorescence measurements, we determine the temperature in the 1031 nm trap to be $T = T_0 R_p^2 = 171 \pm 20$ K. From the damping of the translation motion we obtain a temperature of 140 ± 30 K. Considering that a temperature gradient will exist around the particle and that the particles does not have a regular shape this simple model agrees well with the fluorescence ratio based prediction of 175 K for the temperature in the 1031 nm trap.

Finally, from simple considerations we show that cooling power is sufficient to reduce the temperature of the levitated crystals to those measured in our experiments even in the presence of gas up to pressures 500 mB. In steady state we equate the heating rate due to conduction by gas²⁸ to be equal to the laser refrigeration rate²⁹ and determine a crystal temperature of approximately 200 K (see methods for details). Despite the simplicity of this model it is roughly consistent with the temperatures determined experimentally using the two independent experimental methods outlined above.

We have demonstrated laser refrigeration combined with the isolation provided by levitation to create a levitated nanocryostat whose orientation and rotation can be controlled via the particles' inherent birefringence. Lower temperatures should be achievable using a trapping laser at 1020 nm, operating at lower pressures and using high purity single nanocrystals^{15,30}. Such a system is attractive for optical temperature control of single crystals without the need for traditional large cryostats. $\text{Yb}^{3+}:\text{YLF}$ crystals can also in principle be grown around or bonded to other nanoparticles of interest such as nitrogen vacancy centres contained in diamond³¹. This opens up the possibility for low temperature, high resolution nanoparticle spectroscopy and characterization. As cryogenic cooling is also key for increasing the spin coherence times in solid state systems it will extend the scope of future levitated hybrid optomechanics experiments where both translational and internal temperatures can now be controlled.

References

- ¹ Yin, Z., Li, T., Zhang, X. & Duan, L. Large quantum superpositions of a levitated nanodiamond through spin-optomechanical coupling. *Phys. Rev. A* **88**, 033614 (2013).

- ² Wan, C. *et al.* Free nano-object ramsey interferometry for large quantum superpositions. *Phys. Rev. Lett.* **117**, 143003 (2016).
- ³ Ranjit, G., Cunningham, M., Casey, K. & Geraci, A. A. Zeptonewton force sensing with nanospheres in an optical lattice. *Phys. Rev. A* **93**, 053801 (2016).
- ⁴ Gieseler, J., Quidant, R., Dellago, C. & Novotny, L. Dynamic relaxation of a levitated nanoparticle from a non-equilibrium steady state. *Nat. Nano* **9**, 358 – 364 (2014).
- ⁵ Millen, J., Deesuwana, T., Barker, P. F. & Anders, J. Nanoscale temperature measurements using non-equilibrium brownian dynamics of a levitated nanosphere. *Nat. Nano.* **9**, 425–429 (2014).
- ⁶ Jain, V. *et al.* Direct measurement of photon recoil from a levitated nanoparticle. *Phys. Rev. Lett.* **116**, 243601 (2016).
- ⁷ Li, T., Kheifets, S. & Raizen, M. G. Millikelvin cooling of an optically trapped microsphere in vacuum. *Nat. Phys.* **7**, 527–530 (2011).
- ⁸ Gieseler, J., Deutsch, B., Quidant, R. & Novotny, L. Subkelvin parametric feedback cooling of a laser-trapped nanoparticle. *Phys. Rev. Lett.* **109**, 103603 (2012).
- ⁹ Metcalf, H. J. & van der Straten, P. *Laser Cooling and Trapping of Neutral Atoms* (2007).
- ¹⁰ Pringsheim, P. Zwei bemerkungen über den unterschied von lumineszenz- und temperaturstrahlung. *Zeitschrift für Physik* **57**, 739–746 (1929).
- ¹¹ Mungan, C. E., Buchwald, M. I., Edwards, B. C., Epstein, R. I. & Gosnell, T. R. Laser cooling of a solid by 16 K starting from room temperature. *Phys. Rev. Lett.* **78**, 1030–1033 (1997).
- ¹² Seletskiy, D. V. *et al.* Laser cooling of solids to cryogenic temperatures. *Nat. Photon.* **4**, 161–164 (2010).
- ¹³ Melgaard, S. D., Albrecht, A. R., Hehlen, M. P. & Sheik-Bahae, M. Solid-state optical refrigeration to sub-100 kelvin regime. *Sci. Rep.* **6**, 20380 (2016).
- ¹⁴ Epstein, R. I., Buchwald, M. I., Edwards, B. C., Gosnell, T. R. & Mungan, C. E. Observation of laser-induced fluorescent cooling of a solid. *Nature* **377**, 500–503 (1995).
- ¹⁵ Roder, P. B., Smith, B. E., Zhou, X., Crane, M. J. & Pauzauskie, P. J. Laser refrigeration of hydrothermal nanocrystals in physiological media. *PNAS* **112**, 15024–15029 (2015).
- ¹⁶ Bensalah, A. *et al.* Growth of Yb³⁺-doped YLiF₄ laser crystal by the Czochralski method. Attempt of Yb³⁺ energy level assignment and estimation of the laser potentiality. *Opt. Mater.* **26**, 375 – 383 (2004).
- ¹⁷ Sugiyama, A., Katsurayama, M., Anzai, Y. & Tsuboi, T. Spectroscopic properties of Yb doped YLF grown by a vertical bridgman method. *J. Alloy. Compd.* **408412**, 780 – 783 (2006).
- ¹⁸ Seletskiy, D. V. *et al.* Precise determination of minimum achievable temperature for solid-state optical refrigeration. *J. Lumin.* **133**, 5 – 9 (2013).
- ¹⁹ Singer, W., Nieminen, T. A., Gibson, U. J., Heckenberg, N. R. & Rubinsztein-Dunlop, H. Orientation of optically trapped nonspherical birefringent particles. *Phys. Rev. E* **73**, 021911 (2006).

- ²⁰ Maurice, E., Wade, S. A., Collins, S. F., Monnom, G. & Baxter, G. W. Self-referenced point temperature sensor based on a fluorescence intensity ratio in Yb³⁺-doped silica fiber. *Appl. Opt.* **36**, 8264–8269 (1997).
- ²¹ Collins, S. F. *et al.* Comparison of fluorescence-based temperature sensor schemes: Theoretical analysis and experimental validation. *J. Appl. Phys.* **84**, 4649–4654 (1998).
- ²² Hoang, T. M. *et al.* Torsional optomechanics of a levitated nonspherical nanoparticle. *Phys. Rev. Lett.* **117**, 123604 (2016).
- ²³ Beth, R. A. Mechanical detection and measurement of the angular momentum of light. *Phys. Rev.* **50**, 115–125 (1936).
- ²⁴ Arita, Y., Mazilu, M. & Dholakia, K. Laser-induced rotation and cooling of a trapped microgyroscope in vacuum. *Nat. Comm.* **4**, 2374 (2013).
- ²⁵ Swartzlander, G. A., Peterson, T. J., Artusio-Glimpse, A. B. & Raisanen, A. D. Stable optical lift. *Nat. Photon.* **5**, 48–51 (2011).
- ²⁶ Rings, D., Schachoff, R., Selmke, M., Cichos, F. & Kroy, K. Hot brownian motion. *Phys. Rev. Lett.* **105**, 090604 (2010).
- ²⁷ Blundell, S. & Blundell, C. *Concepts in thermal physics* (Oxford Uni. Press, 2006).
- ²⁸ Liu, F., Daun, K., Snelling, D. & Smallwood, G. Heat conduction from a spherical nano-particle: status of modeling heat conduction in laser-induced incandescence. *Appl. Phys. B-Laser O* **83**, 355–382 (2006).
- ²⁹ Epstein, R. & Sheik-Bahae, M. *Optical Refrigeration in Solids: Fundamentals and Overview*, 1–32 (2009).
- ³⁰ Zhou, X., Smith, B. E., Roder, P. B. & Pauzauskie, P. J. Laser refrigeration of ytterbium-doped sodium-yttrium-fluoride nanowires. *Adv. Mater.* **28**, 8658–8662 (2016).
- ³¹ Neukirch, L. P., von Haartman, E., Rosenholm, J. M. & Vamivakas, A. N. Multi-dimensional single-spin nano-optomechanics with a levitated nanodiamond. *Nat. Photon.* **9**, 653657 (2015).

Acknowledgements

We acknowledge support from the UK's Engineering and Physical Science Research Council grant (EP/N031105/1). We also acknowledge the help of G. W. Morley and A. C. Frangeskou for scanning electron microscopy imaging.

Author contributions

ATM Anishur Rahman & P. F. Barker conceived and designed the experiment. Both authors performed the experiment, analysed the data and have written the manuscript.

Additional information

Correspondence and requests for materials should be addressed to P. F. Barker.

Competing financial interests

The authors declare no competing financial interests.

Methods

Nanocrystal preparation and levitation

Nanocrystals were created from bulk 10% Yb^{3+} :YLF crystal. The manufacturer (Altechna Ltd.) states that all trace impurities $< 0.001\%$. The bulk crystal was milled in an alumina mortar and pestle. The Yb^{3+} :YLF nanocrystals subsequently dispersed in HPLC grade methanol using an ultrasonic bath. A fraction of the solution was added into an asthma nebulizer which was used to introduce the particles into the trapping volume. Once a particle was trapped, the vacuum chamber was evacuated down to pressures as low as 40 mB.

An Elforlight I4-700 Nd:YAG laser operating at a wavelength of 1064 nm and a Lumics diode laser operating at a wavelength of 1031 nm were used to form the optical tweezers trap. The linewidth of the 1064 nm laser was ≈ 10 kHz while the 1031 nm diode laser linewidth, stabilized by a fibre Bragg grating, was quoted by the manufacturer to have a width of ≈ 0.08 nm. The trap was formed by focusing either laser to a spot size (e^{-2} radius) of approximately 400 nm.

Temperature determination from recorded spectra

Fluorescence from levitated nanocrystals, and those deposited on a cover glass, were collected through the same objective lens used for trapping. Spectra were recorded in the wavelength range from 950 to 1000 nm by either a home built spectrometer, consisting of a cooled EMCCD iXon 885 camera from Andor and a 600 lines per mm grating or a SR163i spectrometer equipped with a cooled iDus CCD detector also from Andor. All spectra were corrected for the variation of response as a function of wavelength using a spectrally calibrated quartz tungsten-halogen lamp (QTH10, Thorlabs Ltd). A background spectrum, recorded without the trapped nanocrystal, was subtracted before spectra were corrected for the variation in wavelength response. To remove the strong elastic scattering of the trapping light, a dichroic mirror (DMSP1000, Thorlabs Ltd) and a low pass filter (FESH1000, Thorlabs Ltd) were used. This prevented the recording of spectral features above approximately 1000 nm. Identification of each transition in the recorded spectra are taken from the literature¹⁶. We assumed that there were no strong vibronic transitions within the 950 nm to 1000 nm spectral region.

Differential luminescence thermometry has been successfully utilized to measure the temperature of laser refrigerated bulk crystals^{1,12,18}. However, since we cannot collect fluorescence spectrum of Yb^{3+} ions above 1000 nm due to the response of the short-pass filter and the dichroic mirror that we use, we cannot use this technique. As a result, here we instead determine temperature from the variation in fluorescence intensity with temperature of well defined spectral transitions in Yb^{3+} :YLF^{20,21} assuming thermal equilibrium. This method has been used as a temperature probe using

rare earth doped crystals^{20,21}.

To quantify the temperatures we use the spectral fits and identify the contributions of the three peaks of Yb^{3+} of interest corresponding to transitions $E_5 \rightarrow E_1$ (972 nm), $E_5 \rightarrow E_3$ (993 nm), and $E_6 \rightarrow E_1$ (960 nm). The change in the ratio of the peak areas for each transition can be used to determine the relative population of the E_5 and E_6 levels and hence to find the temperature. Importantly, as we are comparing the same transition at different temperatures, the transition probabilities do not need to be known to determine the temperature from these relative heights provided a reference spectrum at temperature, T_0 is available. For the reference we use a spectrum recorded from the crystal deposited on the cover slip and illuminated with the 1031 nm laser ($T_0 = 295$ K). The temperature of the crystal T can be determined from

$$\frac{1}{T} = \frac{1}{T_0} + \frac{k_B}{\Delta E_{65}} \ln \frac{R_0}{R}, \quad (1)$$

where R is the intensity area ratio of well defined transitions $E_6 \rightarrow E_1$ and $E_5 \rightarrow E_1$ or $E_6 \rightarrow E_1$ and $E_5 \rightarrow E_2$ determined from the fits at temperature T , while R_0 is the same ratio at the room reference temperature taken to be $T_0 = 295$ K from the cover slip data. Additionally, $\Delta E_{65} = E_6 - E_5$, is the energy difference between the E_6 and E_5 states, and k_B is the Boltzmann's constant. For each spectrum we average the two temperatures obtained from the intensity area ratios $\frac{A(E_6 \rightarrow E_1)}{A(E_5 \rightarrow E_1)}$ and $\frac{A(E_6 \rightarrow E_2)}{A(E_5 \rightarrow E_1)}$ described above.

Translational and rotational motion

The translational and rotational motion were detected on a set of balanced photodiodes (PDB210C from Thorlabs Ltd). A time series of this data from the photodiodes was recorded on an oscilloscope and was post processed to extract the power spectral density. The pendular motion and the transverse trap frequency are simultaneously recorded. Fits to the data, assuming damped translational and pendular motion⁸, were used to extract the damping ratios for both types of motion as a function of trapping wavelength. The uncertainties in the damping rates are taken from the standard error derived from a Levenberg-Marquardt fit. This data was used to derive gas temperature which were consistent with those obtained via the fluorescence measurements.

Estimation of equilibrium temperature

The heat transfer rate²⁸ from the nanocrystal to the surrounding gas, in regime where the mean free path of the gas is equal to the particle size, is given by $\dot{q}_h = \frac{8\pi a^2 k_g}{2a + \Lambda G} \Delta T$, where Λ is the mean free path of the air molecules,

$k_g = 0.0257 \text{ Wm}^{-1}\text{K}^{-1}$ is the heat conductivity of dry air and a is the particle radius. The factor G is given by $G = (18\gamma - 10)/A(\gamma + 1)$, where $A = 0.07^{28}$ and $\gamma = 7/2$ are the thermal accommodation coefficient and the specific heat ratio of the air molecules, respectively. The cooling rate from laser refrigeration, ignoring parasitic absorption losses from impurities, is given by $\dot{q}_c = V\alpha I(1 - \eta_q \frac{\lambda}{\lambda_f})$ where V is the nanocrystal volume, α is the temperature dependent absorption coefficient, $I = 3.5 \times 10^{11} \text{ Wm}^{-2}$ is the laser irradiance and $\eta_q \approx 0.995^{12}$ is the quantum efficiency. The absorption coefficient $\alpha = \sigma N_t$ is determined from the absorption cross-section for the bulk crystal at room temperature where $\sigma \approx 1.5 \times 10^{25} \text{ m}^2$ (from the manufacturer data) and $N_t = 1.50 \times 10^{27} \text{ m}^{-3}$ is the number of Yb ions per unit volume for the 10 % doped crystal¹⁷. The excitation wavelength is given by λ while the average emission wavelength is λ_f^{29} . The approximate average emission wavelength $\lambda_f = 997 \text{ nm}$ is determined from the bulk fluorescence spectrum since we do not collect the complete spectrum from the levitated particle due to the short-pass filter and the dichroic mirror that we use. To minimise re-absorption of this fluorescence we collect the fluorescence only near the surface of the crystal where the excitation beam enters it. By equating the heating and cooling rates for a particle of radius $a = 500 \text{ nm}$, we find an equilibrium particle temperature of approximately 200 K using 1031 nm light. We stress that this equilibrium temperature is an estimate since many of the values used in this calculation are approximate and taken from bulk measurements which may differ from those in the nanocrystal.

Data Availability

The data that support the plots within this paper and other findings of this study are available from the corresponding author upon reasonable request.

References

- ¹ Patterson, W. M., Seletskiy, D. V., Sheik-Bahae, M., Epstein, R. I. & Hehlen, M. P. Measurement of solid-state optical refrigeration by two-band differential luminescence thermometry. *J. Opt. Soc. Am. B* **27**, 611–618 (2010).

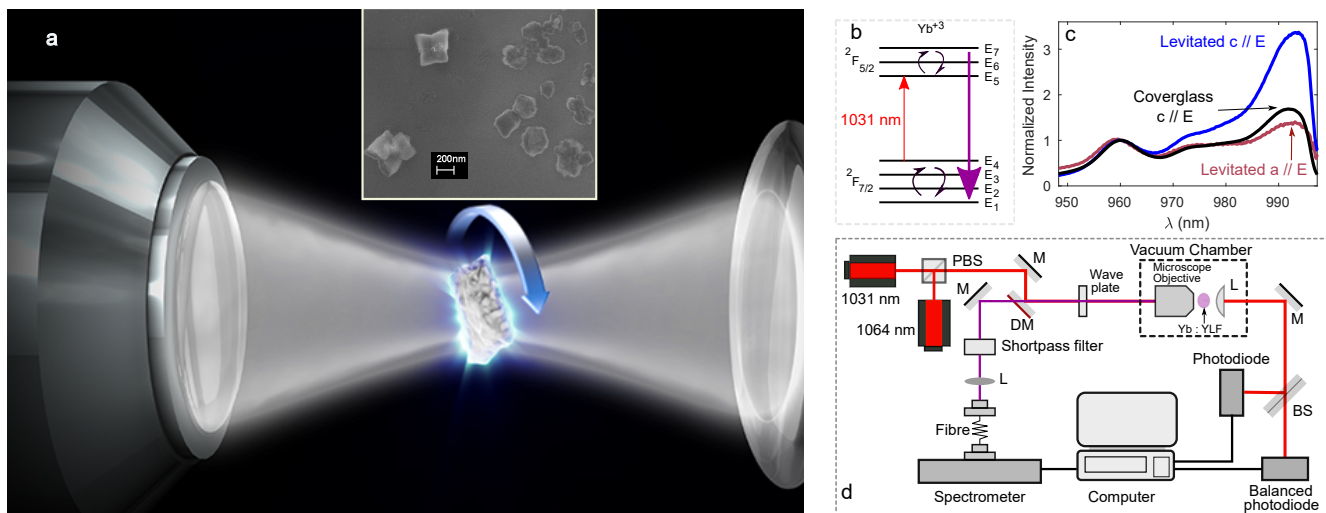


Figure 1: Experimental overview. **a)** Illustration of the levitated $\text{Yb}^{3+}:\text{YLF}$ crystal that is excited by the trapping beam and emitted blue-shifted fluorescence. Inset is a scanning electron microscope image of the nanocrystals used in the experiment. The scale bar is 200 nm. **b)** The energy level diagram of the Yb^{3+} ion within the YLF crystal. Shown is the excitation at 1031 nm and the anti-Stokes fluorescence at shorter wavelengths which lead to internal cooling of the crystal. **c)** Fluorescence spectra obtained from $\text{Yb}^{3+}:\text{YLF}$ nanocrystals under 1031 nm illumination- blue and red solid lines show the spectra from a levitated crystal when its c - and a - axes are parallel to the electric field E of the trapping laser, respectively, while the black solid line represents the spectrum from a $\text{Yb}^{3+}:\text{YLF}$ nanocrystal attached to a microscope coverglass and its c - axis is parallel to the laser's E field. **d)** Optical layout of the experiment : M - mirror, DM - dichroic mirror, PBS - polarizing beam splitter, BS - beam splitter, and L - lens.

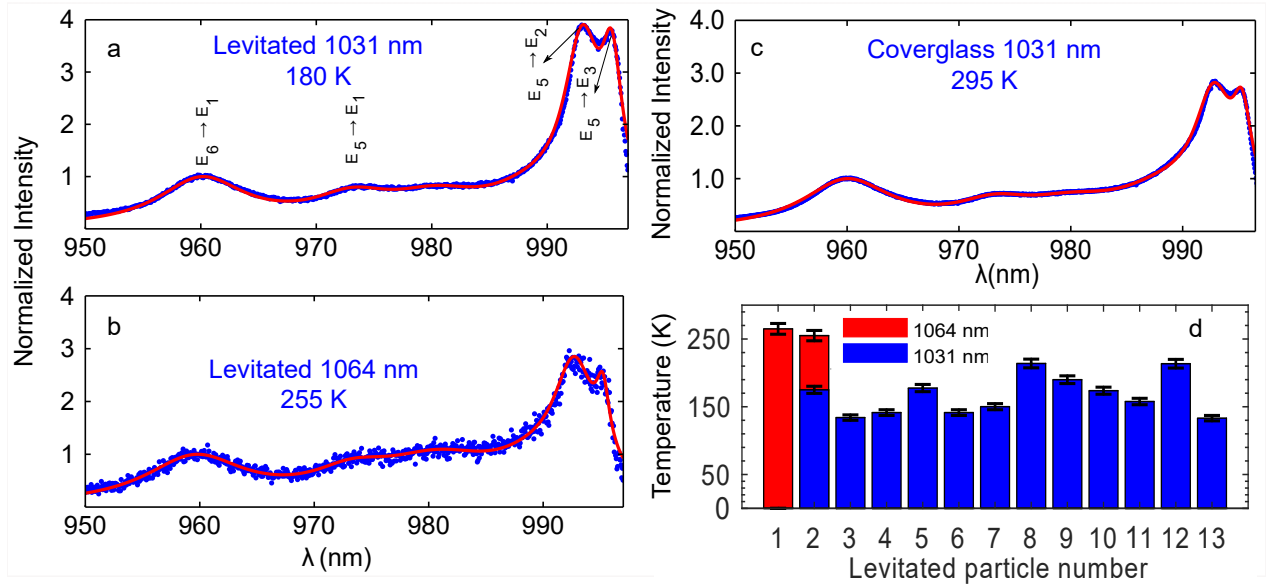


Figure 2: Blue shifted fluorescence from Yb³⁺:YLF nanocrystals in 1031 nm and 1064 nm trapping beams. Red solid lines are fits considering six dominant transitions (Lorentzian profile) of Yb ions in the YLF host. These transitions are modelled as contributions from $E_6 \rightarrow E_1$, $E_5 \rightarrow E_1$, $E_6 \rightarrow E_2$, $E_6 \rightarrow E_3$, $E_5 \rightarrow E_2$, and $E_5 \rightarrow E_3$ transitions, respectively. High resolution spectra from levitated nanocrystals **a)** using 1031 nm and **b)** 1064 nm wavelength levitation. **c)** Fluorescence spectrum from a Yb³⁺:YLF nanocrystal when deposited on a SiO₂ coverglass. Temperatures are determined from the population distribution of the excited state assuming that particles are at room temperature when deposited on a coverglass (see methods section). **d)** A collection of levitated particles and their internal temperatures upon 1031 nm and 1064 nm levitation. Particle 2 was initially trapped using 1031 nm beam and then was gradually transferred to 1064 nm beam while keeping everything else the same. In 1031 nm trapping T was 175 K while that in 1064 nm was 255 K. Fluorescence spectrum of particle number 5 is shown in panel **a**. In this case T is equal to 180 K.

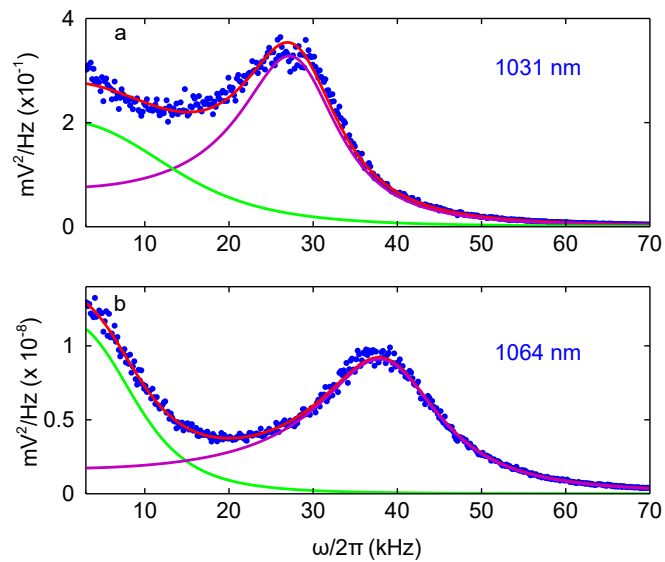


Figure 3: Power spectral density. PSDs corresponding to the pendular motion, oscillation of the elongated particles about the polarization axis of the laser's electric field, of particle number 2 in Fig. 2d at 600 mB **a)** in 1031 nm, and **b)** in 1064 nm trapping, respectively. The blue dots are data points while the red solid lines are fits corresponding to two harmonic oscillators - one for the translational motion (low frequency regime) and the other for the pendular oscillation (around the main peak). From the fit we retrieve the damping Γ that the particle encounters while oscillating in the 1031 nm and 1064 nm traps. As a complementary technique to the fluorescence intensity ratio based thermometry, we find T from $\Gamma \propto \sqrt{T}$ (for more details see text).

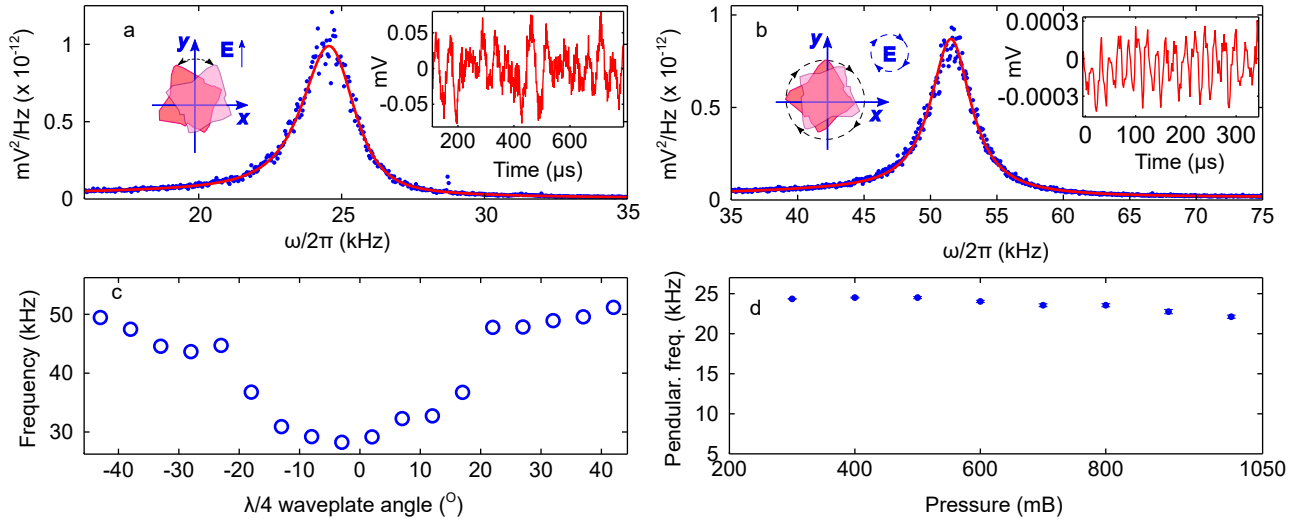


Figure 4: Alignment and rotation of levitated $\text{Yb}^{3+}:\text{YLF}$ particles. **a)** Power spectral density (PSD) of a levitated $\text{Yb}^{3+}:\text{YLF}$ particle at ≈ 500 mB as it performs pendular motion in linearly polarized light. When an asymmetric particle is levitated in linearly polarized light, its long axis is aligned with the direction of polarization. Any misalignment due to collisions with gas molecules is counteracted by the laser field and particles start to perform harmonic oscillation. **b)** PSD of a spinning levitated $\text{Yb}^{3+}:\text{YLF}$ particle in circularly polarized (CP) light at ≈ 500 mB. Due to the inherent asymmetry in the refractive indices along different axes of $\text{Yb}^{3+}:\text{YLF}$ crystal, CP light will also impart torque and rotate the trapped particle. **Insets** are short time traces of the raw data. **c)** Rotational frequency as a function of angle θ on the quarter waveplate. $\theta = 0$ is equivalent to LP light while $|\theta| = 45^\circ$ signifies CP light. $0 < |\theta| < 45$ produces elliptically polarized light and particles rotate at rates in between those at $\theta = 0$ and $|\theta| = 45^\circ$. **d)** Pendular oscillation frequency as a function of pressure.